Evidence for Ferromagnetic Clusters in the Colossal-Magnetoresistance Material EuB_6

Merlin Pohlit,[1] Sahana Rößler,[2] Yuzo Ohno,[3,*] Hideo Ohno,[3] Stephan von Molnár,[4] Zachary Fisk,[5] Jens Müller,[1,†] and Steffen Wirth[2]

[1]*Institute of Physics, Goethe-University Frankfurt, 60438 Frankfurt (M), Germany*
[2]*Max-Planck-Institute for Chemical Physics of Solids, 01187 Dresden, Germany*
[3]*Research Institute of Electrical Communication, Tohoku University, Sendai 980-8577, Japan*
[4]*Department of Physics, Florida State University, Tallahassee, Florida 32306, USA*
[5]*Department of Physics, University of California, Irvine, California 92697, USA*

(Received 20 November 2017; revised manuscript received 13 April 2018; published 19 June 2018)

We combined scanning tunneling microscopy and locally resolved magnetic stray field measurements on the ferromagnetic semimetal EuB_6, which exhibits a complex ferromagnetic order and a colossal magnetoresistance effect. In a zero magnetic field, scanning tunneling spectroscopy visualizes the existence of local inhomogeneities in the electronic density of states, which we interpret as the localization of charge carriers due to the formation of magnetic polarons. Micro-Hall magnetometry measurements of the total stray field emanating from the end of a rectangular-shaped platelike sample reveals evidence for magnetic clusters also in finite magnetic fields. In contrast, the signal detected below the faces of the magnetized sample measures a local stray field indicating the formation of pronounced magnetic inhomogeneities consistent with large clusters of percolated magnetic polarons.

DOI: 10.1103/PhysRevLett.120.257201

Materials in which the electronic and magnetic properties of the system are strongly modified by the exchange coupling between the conduction electrons and local magnetic moments are of fundamental importance in modern condensed-matter physics as well as of technological interest, e.g., in spintronics research [1]. A manifestation of this effect is, for example, the emergence of a large negative or even colossal magnetoresistance (CMR) observed in various types of magnetic semiconductors, rare-earth chalcogenides and hexaborides, Mn-based pyrochlores, and mixed-valent rare-earth perovskite manganites [2–5]. In these materials, a universal tendency to form intrinsic (i.e., nonchemical) inhomogeneous states is often observed, see, e.g. [6,7], which is related to the formation of ordered magnetic clusters, or magnetic polarons (MP). Such objects evolve as a result of a large exchange interaction between the conduction electrons and the localized spins, i.e., when it is energetically favorable for the charge carriers to localize while spin-polarizing the local magnetic moments over a finite distance given by the localization length of the charge carriers. A percolation transition of MP, resulting in a delocalization or sudden mobility increase of the charge carriers once the magnetic clusters overlap, is an intriguingly simple model for explaining the CMR effect in many of these materials [8–12].

For the present study, in which we aim to (i) visualize the electronic phase separation and (ii) find evidence for magnetic cluster formation in finite magnetic fields, we have chosen the ferromagnetic semimetal EuB_6 [13], which, due to its simple lattice and magnetic structure, may be viewed as a "clean" model system for studying purely spin-tuned transport phenomena. Because Eu^{2+} is an ${}^8S_{7/2}$-state ion with a large magnetic moment of (theoretically) $\mu_{\mathrm{eff}} = 7.94\ \mu_B$, the magnetic properties are isotropic and apparently particularly simple. The transition into the ferromagnetic state, however, shows an intriguingly complex behavior with two consecutive transitions at about $T_{c_1} = 15.3$ K and $T_{c_2} = 12.6$ K [11,14–17]. Reminiscent of the behavior of the mixed-valent manganites, the paramagnetic-to-ferromagnetic transition is accompanied by a drastic reduction of the resistance in zero magnetic field as well as a CMR effect in finite magnetic fields, which is strongest around T_{c_1}. It has been proposed that this large negative MR in EuB_6 at T_{c_1} is related to a percolation-type transition resulting from the overlap of MP, which causes a delocalization of the hole carriers [10,11,18]. MP commence to form at a temperature scale $T^* \sim 35$–40 K [11,12,14,15] and upon cooling or increasing magnetic field grow in size and/or number until they percolate (form links) at $T \leq T_{c_1}$. These polaronic clusters finally merge at $T \leq T_{c_2}$, where bulk ferromagnetic order sets in—a scenario in accordance with recent transport data [14,18]. In μSR experiments, two distinct and spatially separate regions associated with different magnetic behavior have been observed upon cooling through the transitions at T_{c_1} and T_{c_2}, providing evidence for magnetic phase separation that can be interpreted in terms of the gradual coalescing of magnetic polarons [19].

In an effort to directly visualize the polaron formation, we conducted spectroscopy by utilizing scanning tunneling

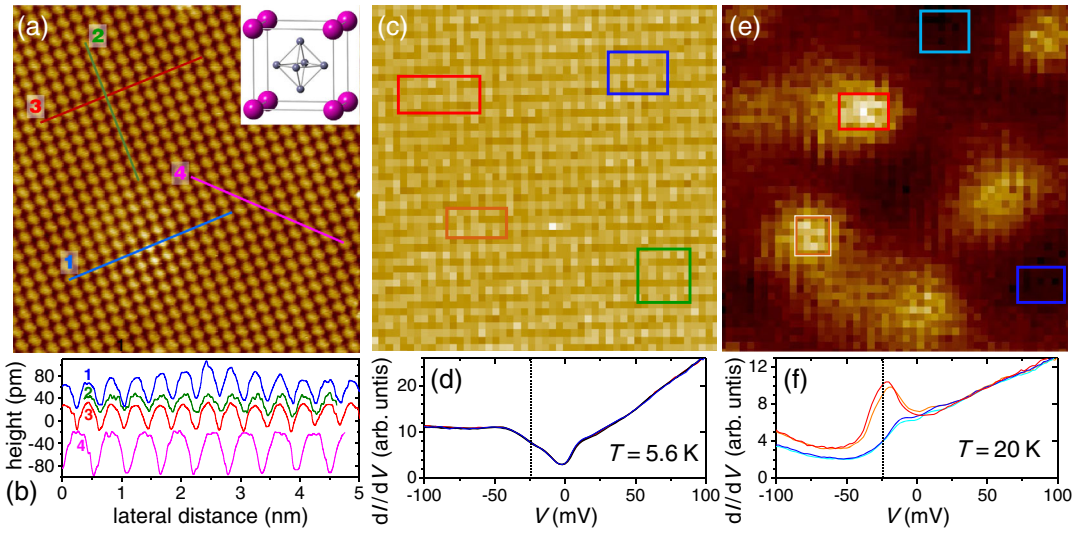

FIG. 1. (a) Topography of EuB_6 over an area of 10 nm × 10 nm ($V = -0.2$ V, $I_{sp} = 0.5$ nA). Inset: cubic crystal structure of EuB_6. (b) Height scans along the lines marked in (a). (c),(e) Maps of local conductance $g(V) = dI(V, \vec{r})/dV$ at $V = -24$ mV over an area of 20 nm × 20 nm obtained at 5.6 K (c) and 20 K (e). At 5.6 K, the EuB_6 surface is nearly homogeneously conducting, while at 20 K local inhomogeneities are clearly visible. (d),(f) $dI(V)/dV$-spectra averaged within areas marked in (c) and (e), respectively, by rectangles of corresponding colors. In (d), a curve averaged over the total area is also included. The local inhomogeneities are most pronounced at $V = -24$ mV, dashed lines in (d) and (f).

microscopy (STM) and spectroscopy (STS) in an ultrahigh vacuum system [20]. This allows us to study the evolution of the local density of states (DOS) at an atomically resolved length scale at different temperatures. Figure 1(a) presents a zoom into a (10×10) nm^2 field of view, see also [21]. The distance between the corrugations is 0.41 nm, Fig. 1(b), in excellent agreement with the lattice constant $a = 0.4185$ nm. Note that line 2 is oriented almost perpendicular to the fast scan direction which causes a slightly enhanced noise of this line compared to lines 1 and 3. The square arrangement of the corrugations aligned parallel to the main crystallographic directions $\langle 100 \rangle$ and $\langle 010 \rangle$, respectively, is expected for the cubic CaB_6 structure type (space group $Pm\bar{3}m$), see inset to Fig. 1(a), and manifests the absence of any severe surface reconstruction. Importantly, no interjacent corrugations were observed between the main ones, see line 4 parallel to a $\langle 110 \rangle$ direction: additional, less pronounced corrugations stemming from the apex of the B octahedra have characterized the Sm-terminated surfaces of SmB_6 [22]. By analogy, we therefore suggest Fig. 1(a) to represent a B-terminated surface, in which case even the corrugation height and the appearance of slight inhomogeneities (line 1) are in concert with the findings on SmB_6 [22].

The tunneling conductance $g(V) = dI(V)/dV$ is, within simplifying approximations, proportional to the local DOS. Details of our tunneling measurements can be found in the Supplemental Material (SM) [21]. Representative results obtained at $T = 5.6$ and 20 K are compared in Figs. 1(c)–1(f) (see the SM [21] for data at an intermediate temperature $T_{c_2} < T = 15\ \mathrm{K} < T_{c_1}$). Locally resolved maps of $g(V, \vec{r})$ at constant $V = -24$ mV for the two temperatures are presented, respectively, in (c) and (e), while area-averaged $g(V)$ curves for the same T are given in (d) and (f). The respective areas for averaging are marked in the maps (c) and (e). We note that in Fig. 1(d), i.e., at $T = 5.6$ K, also a curve averaged over the total area of (c) is included emphasizing negligible spatial inhomogeneities of the DOS deep inside the ferromagnetically ordered phase.

In contrast, the spectroscopic findings in the paramagnetic state at $T = 20$ K are markedly different. Here, local inhomogeneities are obvious, specifically for negative bias voltage V. The locally resolved map, Fig. 1(e), taken at $V = -24$ mV, visualizes areas of increased DOS of about 3–4 nm in extent (this size does not depend on V). The conductivity curves, Fig. 1(f), reveal a clearly resolved peak at around $V = -24$ mV within these areas, while no inhomogeneities are found (i.e., the $dI(V, \vec{r})/dV$ curves match up nicely) for $V \lesssim -200$ mV and $V \gtrsim 0$ mV. We interpret this as the localization of charge carriers due to the formation of polarons. Note that in the manganites such polarons of very similar size have been visualized by STM, see, e.g., [23].

After having established nanoscale inhomogeneities in the local DOS, we provide evidence for the existence of magnetic clusters also in finite magnetic fields. To that end, micro-Hall magnetometry is employed, which allows for the local detection of the magnetic stray field emanating from a sample on top of an ultra-sensitive Hall sensor composed of five adjacent Hall crosses of size 10 μm × 10 μm. A rectangular-shaped thin slab of EuB_6 with

dimensions 457 μm × 91 μm × ~15 μm and smooth surfaces was chosen to minimize inhomogeneities of the sample magnetization due to demagnetization effects, see SI [21], which includes Refs. [24,25]. The measured Hall voltage V_H is, in first approximation, given by $V_H = (1/ne) \times I \times \langle B_z \rangle$, where I denotes the current through the Hall sensor, n its carrier concentration, and $\langle B_z \rangle$ the sample's magnetic stray field component perpendicular to the sensor plane averaged over the active area of the Hall cross. The sensor plane is aligned parallel to the external field.

The EuB_6 sample was positioned on top of the Hall crosses in a way that two extreme cases are realized simultaneously and allow for comparison: cross A is located right underneath one end of the sample, while cross B is entirely covered as depicted schematically in the inset of Fig. 2(a). Cross A is penetrated by the total stray field emanating from magnetic surface charges at the sample's face and therefore is proportional to its total magnetization. This is confirmed by an excellent scaling of the measured Hall voltage at various different external magnetic fields to the magnetization measurements using a commercial SQUID magnetometer reported in [18]. Selected stray field measurements at the position of cross A are presented in Fig. 2(a). At high enough fields, demagnetization effects which would result in pronounced inhomogeneous magnetic states can be neglected. Hence, $\langle B_z \rangle$ is a measure of the sample's magnetization M, and we fit the $\langle B_z \rangle$ vs T curves taken at cross A with the following classical mean-field expression [26,27]:

$$\frac{M}{M_s} = \mathcal{L}(\alpha) \equiv \coth(\alpha) - \frac{1}{\alpha}, \tag{1}$$

with

$$\alpha = \frac{\mu B_{\text{ext}}}{k_B T} + 3\frac{T_C}{T}\frac{M}{M_s}. \tag{2}$$

In this model, instead of using the Brillouin function with fixed magnetic moment, the Langevin description allows for considering magnetic clusters [26], in our case related to the formation of MP. The three free parameters of the fits are (i) the mean-field saturation moment M_s, corresponding to the saturation stray field $\langle B_z \rangle_{\text{sat}}$, (ii) the ferromagnetic mean-field Curie temperature T_C, for which in our case $T_C = T_{c_2}$, and (iii) the mean-field magnetic moment μ (in units of μ_B) associated with the individual magnetic clusters whose internal degrees of freedom are considered frozen. The fits based on the simple model of Eqs. (1) and (2) shown as dashed lines in Fig. 2(a) reproduce the measured data very well for $B_{\text{ext}} \geq 75$ mT. As a consistency check, we show in Fig. 2(c) that the transition temperatures T_C obtained from the model agree with T_{c_2}. Although the $\langle B_z \rangle(T)$ curves are well described individually, we find that

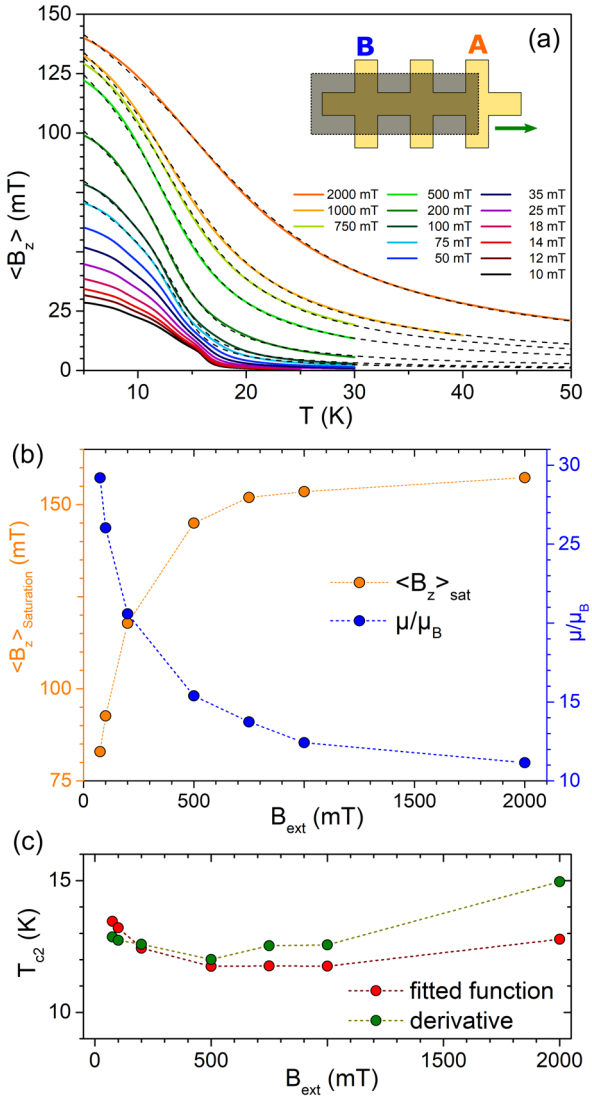

FIG. 2. (a) Temperature-dependent magnetic stray field $\langle B_z \rangle$ vs T (solid lines) detected at cross A (see schematics in the inset) in external magnetic fields $B_{\text{ext}} \geq 10$ mT. Dashed lines are three-parameter fits of a mean-field magnetization model, Eqs. (1) and (2), as described in the text. Fit parameters (b) saturation stray field $\langle B_z \rangle_{\text{sat}} \propto M_s$ and cluster size μ/μ_B, and (c) transition temperature T_C in dependence on B_{ext} compared to T_{c_2} as determined from the peak in the derivative of the $\langle B_z \rangle(T)$ curves shown in (a).

the fitting parameters $\langle B_z \rangle_{\text{sat}}$ and μ are strongly field dependent. Such a behavior has also been observed for thin-film samples of manganites and was interpreted as suggestive of magnetic nanoclusters, the total magnetic moment of which is strongly field dependent [27]. The observed field dependence of the saturation moment $M_s \propto \langle B_z \rangle_{\text{sat}}$, see Fig. 2(b), suggests that for larger magnetic fields, the ferromagnetic ordering of EuB_6 is stronger. The fitting parameter T_C, however, roughly stays constant, in contrast to the findings for manganite thin films, where it strongly increases [27]. The effective cluster moment

reaches $\mu \sim 11\mu_B$ at 2 T exhibiting a tendency toward saturation; i.e., the system becomes more homogeneous and approaches the expected value of $\sim 8\mu_B$ of the individual Eu^{2+} spins of one unit cell. The larger values of μ for lower fields suggests the existence of larger magnetic clusters resulting in a transition in $M(T)$ that is substantially broader than expected from simple mean-field theory in small fields. At $B_{\mathrm{ext}} = 75$ mT, the lowest field where the influence of the transition at T_{c_1} as well as demagnetization effects can safely be neglected, the fit yields $\mu \approx 30\ \mu_B$ corresponding to roughly four times the value of the magnetic moment of one unit cell [28]. We suggest that the magnetic clusters, which lead to a substantially broadened magnetization behavior in finite magnetic fields, are the same objects, namely, the magnetic polarons, that are observed in STM in zero field.

Finally, we discuss marked differences of the total and local stray fields detected at crosses A and B, respectively, near the percolative transition at T_{c_1}, in particular, at smaller externally applied magnetic fields. In comparison to cross A, the perpendicular component of the magnetic stray field detected underneath the sample (e.g., at cross B), in the case of the magnetization lying along the long axis of the specimen, is expected to be much smaller (or even zero). Yet, these crosses are sensitive to perpendicular stray field components below the sample caused by inhomogeneities of the sample's magnetization, which may allow the detection of local effects stemming from percolated magnetic clusters. The contour plots Figs. 3(a) and 3(b) compare the temperature-dependent magnetic stray field measurements for the crosses A and B, respectively. Clearly, for cross B, we observe a pronounced additional

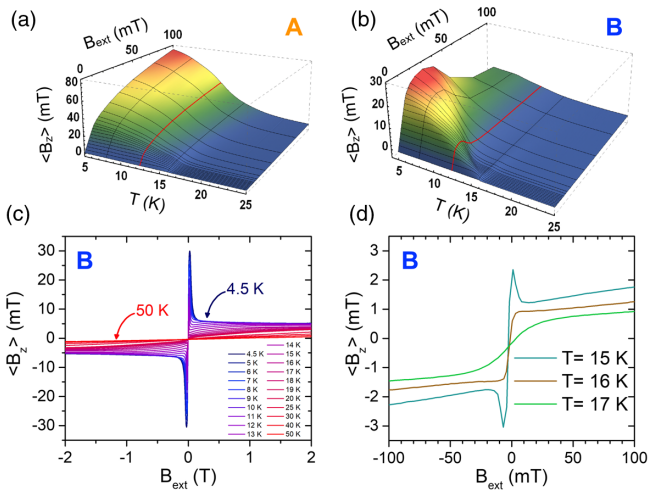

FIG. 3. (a),(b) Total and local magnetic stray fields detected at crosses A and B, respectively, as contour plots $\langle B_z \rangle (T, B)$. Red lines are selected curves $\langle B_z \rangle (B_{\mathrm{ext}}, T = \mathrm{const})$. (c) Field-sweep data of cross B in a wider field range at various constant temperatures. (d) Enlarged diagram of selected temperatures showing the occurrence of the characteristic peak below T_{c_1}.

stray field contribution. The difference between the detected stray fields at crosses A and B becomes obvious upon considering curves $\langle B_z \rangle (B_{\mathrm{ext}}, T = \mathrm{const})$, see red lines in the contour plots. The total stray field caused by the sample's volume magnetization (cross A) shows the expected linear behavior in the paramagnetic regime at elevated temperatures that changes towards S-shaped curves, indicating the onset of ferromagnetic ordering when cooling through T_{c_1}. In contrast, at cross B a strong perpendicular stray field component gives rise to a pronounced sharp peak at small external fields, which sets in below T_{c_1}, as shown in Figs. 3(c) and 3(d), indicating a peculiar spatial distribution of the local magnetic induction (for the magnetic field dependence of T_{c_1}, see the SM [21], which includes Ref. [29]). Two possible explanations are obvious. It is conceivable that this strong perpendicular component of the stray field below the sample is caused by the formation of a conventional magnetic domain structure. However, considering that EuB_6 is a rather soft magnetic material and that the bulk magnetic order sets in below T_{c_2} [11] and not T_{c_1}, we suggest as an alternative explanation that the observed behavior is caused by magnetic phase separation due to the percolation of MP in small external fields where a large connected (or "infinite") cluster of linked MP forms below T_{c_1}. This in turn corresponds to pronounced ferromagnetic inhomogeneities. Because of the overlap of MP, a considerable part of $\sim 15\%$ of the Eu^{2+} spins become magnetically ordered already at T_{c_1} [11,15] and aligned in the preferred direction given by the percolation path, which forms an "intrinsic" anisotropy, determined by the free-energy landscape of the sample. This is essentially equivalent to a stable magnetic domain giving rise to the strong peak in $\langle B_z \rangle (B_{\mathrm{ext}})$. It is reasonable to assume that for increasing external fields the magnetic moments of the cluster network become increasingly aligned with the field direction and merge with the surrounding remaining paramagnetic spins. This increasing homogeneity and directional change naturally explains the observed suppression of the local stray field as the sample magnetization approaches saturation, see Fig. 3(c), whereas it is noteworthy that the inhomogeneities causing the observed peak in $\langle B_z \rangle (B_{\mathrm{ext}})$ still persist in the ferromagnetic phase below T_{c_2}.

In summary, we were able to visualize nanoscale clusters in the electronic density of states in STM/STS measurements in a zero magnetic field and at a temperature above the ferromagnetic transition, which are absent deep in the magnetically ordered phase. In small magnetic fields, the local magnetic stray field detected below the magnetized sample signifies the existence of large magnetic clusters that can be interpreted in terms magnetic phase separation and the percolation of magnetic polarons. In higher magnetic fields, the total magnetic stray field emanating from the sample end shows a significant field-dependent broadening of the bulk ferromagnetic transition. A classical

mean-field analysis in the more homogenous magnetization state in large fields indicates a cluster size of the order of a few unit cells.

M. P. and J. M. acknowledge technical support from A. Amyan. S. R. and S. W. acknowledge support by the DFG through SPP 1666.

*Present address: Faculty of Pure and Applied Sciences, University of Tsukuba, Tsukuba, Japan.
†j.mueller@physik.uni-frankfurt.de

[1] Y. Tokura, M. Kawasaki, and N. Nagaosa, Nat. Phys. **13**, 1056 (2017).
[2] S. von Molnár and S. Methfessel, J. Appl. Phys. **38**, 959 (1967).
[3] A. P. Ramirez and M. A. Subramanian, Science **277**, 546 (1997).
[4] *Colossal Magnetoresistance, Charge Ordering and Related Properties of Manganites*, edited by C. N. R. Rao and B. Raveau, (World Scientific, Singapore, 1998).
[5] A. Kaminski and S. Das Sarma, Phys. Rev. Lett. **88**, 247202 (2002).
[6] M. Uehara, S. Mori, C. H. Chen, and S.-W. Cheong, Nature (London) **399**, 560 (1999).
[7] E. Dagotto, T. Hotta, and A. Moreo, Phys. Rep. **344**, 1 (2001).
[8] S. von Molnár, Sens. Actuators A **91**, 161 (2001).
[9] J. M. De Teresa, M. R. Ibarra, P. A. Igarabel, C. Ritter, C. Marquina, J. Blasco, J. Garcia, A. del Moral, and Z. Arnold, Nature (London) **386**, 256 (1997).
[10] P. Nyhus, S. Yoon, M. Kauffman, S. L. Cooper, Z. Fisk, and J. L. Sarrao, Phys. Rev. B **56**, 2717 (1997).
[11] S. Süllow, I. Prasad, M. C. Aronson, S. Bogdanovich, J. L. Sarrao, and Z. Fisk, Phys. Rev. B **62**, 11626 (2000).
[12] U. Yu and B. I. Min, Phys. Rev. B **74**, 094413 (2006).
[13] Z. Fisk, D. C. Johnston, B. Cornut, S. von Molnár, S. Oseroff, and R. Calvo, J. Appl. Phys. **50**, 1911 (1979).
[14] P. Das, A. Amyan, J. Brandenburg, J. Müller, P. Xiong, S. von Molnár, and Z. Fisk, Phys. Rev. B **86**, 184425 (2012).
[15] R. S. Manna, P. Das, M. de Souza, F. Schnelle, M. Lang, J. Müller, S. von Molnár, and Z. Fisk, Phys. Rev. Lett. **113**, 067202 (2014).
[16] S. Süllow, I. Prasad, M. C. Aronson, J. L. Sarrao, Z. Fisk, D. Hristova, A. H. Lacerda, M. F. Hundley, A. Vigilante, and D. Gibbs, Phys. Rev. B **57**, 5860 (1998).
[17] R. R. Urbano, P. G. Pagliuso, C. Rettori, S. B. Oseroff, J. L. Sarrao, P. Schlottmann, and Z. Fisk, Phys. Rev. B **70**, 140401(R) (2004).
[18] X. Zhang, L. Yu, S. von Molnár, Z. Fisk, and P. Xiong, Phys. Rev. Lett. **103**, 106602 (2009).
[19] M. L. Brooks, T. Lancaster, S. J. Blundell, W. Hayes, F. L. Pratt, and Z. Fisk, Phys. Rev. B **70**, 020401(R) (2004).
[20] Omicron Nanotechnology GmbH, Taunusstein, Germany.
[21] See Supplemental Material at http://link.aps.org/supplemental/10.1103/PhysRevLett.120.257201 for details of the STS and magnetic stray field experiments. Furthermore, STS data at intermediate temperatures and stray field data at small external fields are discussed.
[22] S. Rößler, T.-H. Jang, D. J. Kim, L. H. Tjeng, Z. Fisk, F. Steglich, and S. Wirth, Proc. Natl. Acad. Sci. U.S.A. **111**, 4798 (2014).
[23] H. M. Rønnow, Ch. Renner, G. Aeppli, T. Kimura, and Y. Tokura, Nature (London) **440**, 1025 (2006).
[24] E. Kneller, *Ferromagnetismus* (Springer, Berlin-Göttingen-Heidelberg, 1962).
[25] J. Müller, Y. Li, S. von Molnár, Y. Ohno, and H. Ohno, Phys. Rev. B **74**, 125310 (2006).
[26] J. I. Gittleman, Y. Goldstein, and S. Bozowski, Phys. Rev. B **5**, 3609 (1972).
[27] J. Z. Sun, L. Krusin-Elbaum, A. Gupta, G. Xiao, and S. S. P. Parkin, Appl. Phys. Lett. **69**, 1002 (1996).
[28] It is important to note that—unlike in MP percolation models [5]—in the model [(Eqs. (1) and (2)] used for fitting the data $\langle B_z \rangle$ vs T in Fig. 2, a temperature-independent moment of the clusters is assumed, a necessity to limit the number of free parameters. This, and neglecting a possible influence of the background surrounding the clusters, is an oversimplification even in larger external fields where the percolation at T_{c_1} is already strongly suppressed. Still, the obtained effective cluster moment qualitatively captures the system's changes from an inhomogeneous low-field state to a more homogeneous state in higher magnetic fields. As a possible explanation, we suggest a "softening" of the magnetic clusters/MP, i.e., a breakdown of the concept of individual MP due to the increasing polarization of the paramagnetic background in strong external fields.
[29] A. Amyan, P. Das, J. Müller, and Z. Fisk, J. Korean Phys. Soc. **62**, 1489 (2013).